X-ray Microdiffraction Study of Chain Orientation in Poly(*p*-phenylene terephthalamide)

Christian Riekel* and Thomas Dieing

European Synchrotron Radiation Facility, B.P. 220, F-38043 Grenoble Cedex, France

Per Engström

KCK, Chalmers University of Technology, S-41296 Göteborg, Sweden

Laszlo Vincze

University of Antwerp, Department of Chemistry, Universiteitsplein, B-2610 Wilrijk-Antwerp, Belgium

Chris Martin and Arumugam Mahendrasingam

Department of Physics, Keele University, Staffs ST5 5BG, U.K.

Received February 23, 1999; Revised Manuscript Received September 7, 1999

ABSTRACT: Single fibers of poly(*p*-phenylene terephthalamide) (PPTA; trade names: Kevlar^{29}, Kevlar^{49}, and Kevlar^{149}) have been scanned through a 3 μm diameter X-ray beam and the degree of orientation (f_c) determined at every point. All samples show a gradient in f_c values from the skin to the core. The highest degree of orientation was found at the edges of the fibers. This effect is particularly strong for Kevlar^{29}. In addition, ripples in orientation were observed along the fiber axis for Kevlar^{29}, but on a smaller scale than the transversal gradient. Upon tensile deformation up to about 3 GPa applied stress, the transversal f_c anisotropy is gradually reduced and disappears at the highest stress values. Kevlar^{29} attains at about 1.5 GPa applied stress the same degree of orientation as Kevlar^{49}.

Introduction

Poly(*p*-phenylene terephthalamide) (PPTA) forms high-strength, high modulus fibers[1−3] which show a fibrillar hierarchy.[4] X-ray diffraction experiments on PPTA fibers show that the size and orientation of the coherently scattering, anisotropic domains is modified by the processing conditions.[5,6] The orientation of the crystalline domains along the fiber axis and therefore of the molecular chains which form the microfibrils[4] has been correlated with mechanical properties such as the tensile modulus.[2,7−9] Experimental data were obtained from whole fibers or fiber bundles. It is, however, of interest to know the variation of this orientation across a single fiber in order to develop more refined microscopic models for the mechanical properties and mechanism of failure. Although electron diffraction techniques can provide local structural information, it is practically impossible to correlate multiple thin fiber sections in order to get information on the whole fiber. Scanning X-ray microdiffraction with beam sizes of a few micrometers allows, however, the recording of high-quality wide-angle X-ray scattering (WAXS) patterns from single fibers as shown for PPTA and ultrahigh molecular weight polyethylene.[10] This method will be extended in the present paper to single PPTA fibers at different degrees of strain with the main aim of determining the extent of variation of crystalline domain orientation within single fibers.

The paper is organized in the following way: (i) samples and methods are introduced in the Experimental Section, and (ii) the methods are first applied to unstrained PPTA fibers and (iii) extended to fibers undergoing tensile strain.

Experimental Section

Materials. K. Gardner (DuPont, Wilmington, DE) provided PPTA fibers (trade names Kevlar^{29}, Kevlar^{49}, and Kevlar^{149}). In the following article, the trade names will be used to designate a specific PPTA fiber. The abbreviation Kevlar^{29,49,149} indicates three different fibers of Kevlar^{29}, Kevlar^{49}, and Kevlar^{149}. The fiber diameters were determined by scanning electron microscopy (SEM) as follows: Kevlar^{29}, 11.6 μm; Kevlar^{49}, 10.7 μm; Kevlar^{149}, 10.8 μm.

X-ray Diffraction. Single fibers were selected under an optical microscope and glued to the support structure by fast glue. The support structure was a steel ring for experiments without applied stress. The stretching cell is described below.

X-ray diffraction experiments were performed at the ESRF microfocus beamline at a wavelength of 0.0782 nm (Si-111 monochromator) using a 3 μm diameter beam (full width) from a glass capillary.[10] Experiments were performed in air at $T = 25.0 \pm 0.5$ °C. The fiber axis was oriented in the vertical direction and normal to the X-ray beam. A specific point of the sample was aligned in a high-resolution optical microscope and then transferred into the center of the X-ray beam at the exit of the capillary by a three-axis gantry which was interfaced by a computer-controlled motion software. Positioning of different samples in the X-ray beam was reproducible to about 2 μm. The sample was step scanned through the beam covering a 11(h) × 11(v) mesh with 2 μm horizontal and 5 μm vertical steps. At every position of the mesh, a frame (2D-diffraction pattern) was recorded in transmission for 30 s using a 130 mm diameter entrance window CCD detector (MAR; 64.45 × 64.45 μm^2 pixels; 16-bit readout; ≈4 s readout time/frame). The detector-to-sample distance was determined by an Al_2O_3 calibration standard as $D = 41.58$ mm. The distance of a fiber relative to the detector was constant to $\Delta D/D \approx 2 \times 10^{-4}$ for the different fibers studied. A typical mesh scan took about 70 min to record. In the present case, data analysis was limited to the strongest equatorial reflections (see below). Matching the framing-time to the intensity of the strongest

10.1021/ma990267m CCC: $18.00 © 1999 American Chemical Society
Published on Web 10/27/1999

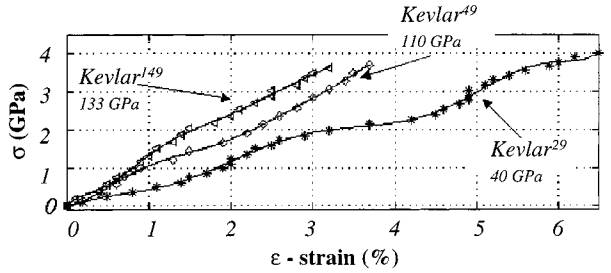

Figure 1. Stress/strain curves of single Kevlar[29,49,149] fibers. The zero point of the abscissa has been defined by a linear extrapolation of the first part of the stress/strain curve to $\sigma = 0$ (GPa). The strain rate was about 5% min^{-1}. Tensile modulus in fiber direction ($E_{||}$) are derived from the initial rise of the curves.

equatorial reflections (see below) and using a 12-bit CCD with 0.1 s readout time could therefore considerably increase the data collection rate.

Stretching Experiments. The stretching cell, based on a slit system with flexure hinges and a piezo actuator (Piezosysteme Jena), was modified for fiber stretching experiments.[11] An improved version of this cell, used in the present work, was developed by a Keele/ICI/ESRF collaboration for micro small-angle X-ray scattering.[12] In addition to the original design it incorporated an Entran strain gauge (0.5 N range) and a homemade tension control. The ends of a single fiber were twisted around half cylinders, which were fixed on the two yaws of the stretching cell. The fiber-ends were glued to the half cylinders by cyanoacrylate glue (Loctite 401) and cured for several hours at room temperature. Care was taken to minimize diffusion of the glue along the fiber. The distance between the attachment points on the half cylinders (L), which could be symmetrically increased up to $L + \Delta l$ ($\Delta l \leq 230$ μm), was calibrated optically. Stress values were recorded before and after each experiment. Values indicated below correspond to average values. Some tests were also made with a further stretching cell, developed at ESRF, with $\Delta l \leq 280$ μm and a direct control of strain (ϵ) through a computer interface. Stress/strain curves obtained for single Kevlar[29,49,149] fibers, measured at an average strain rate of about 0.5% min^{-1}, are shown in Figure 1. Tensile moduli in the fiber direction ($E_{||}$) of ≈40 GPa (Kevlar[29]), ≈110 GPa (Kevlar[49]), and ≈133 GPa (Kevlar[149]) were determined from the initial rise of the curves. A yield point appears below ≈1% strain. Similar stress/strain curves for PPTA fibers have been reported in the literature.[2] The initial rise has been explained by an extension of the fibrillar structure while rupture of hydrogen bonds and a progressive contraction of the orientation distribution has been proposed for higher strains.[2,13] It should be noted that the slopes and therefore the tensile modulus of the different samples in Figure 1 become comparable before rupture. Comparable orientation distributions would therefore be expected. We have yet to test the repeatability of such stress/strain curves on a larger amount of single fibers.

For X-ray diffraction experiments the stretching cell was fixed on an eucentric Huber goniometer head. Experimental conditions for sample alignment were identical with experiments on fibers without applied stress. The number of mesh scans performed per sample was four to five, up to a stress of about 3 GPa, which is yet too limited for a more detailed study of the stress/strain curves (Figure 1). Fibers broke in general above about 3 GPa.

The sample to detector distance was calibrated by a Si powder calibration standard to $D = 39.44$ mm. The stretching cell was not moved along the beam path during the stretching experiments. Because of the measuring time of about 70-min per mesh scan, creep values of the stress were about 10%.

Data Reduction and Modeling. Data reduction for the selected patterns was performed with the FIT2D software package.[14] For background subtraction, patterns were scaled to a common region of interest dominated by background scattering. For recursive fitting of Gaussian or Lorentzian

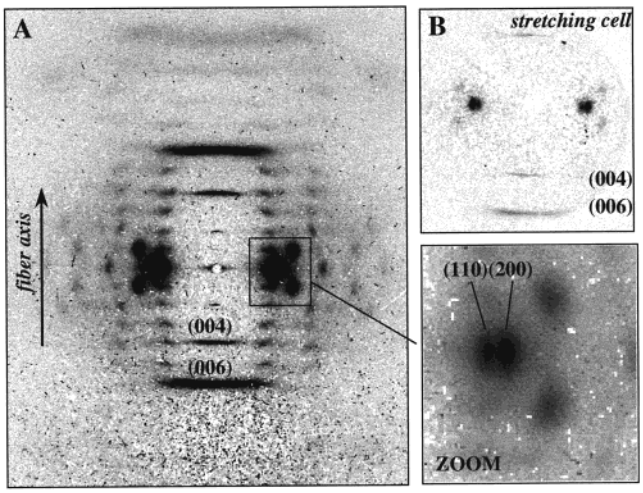

Figure 2. (A) Diffraction pattern of Kevlar[49] fiber. The lower part of the pattern is shadowed by the sample support. Intensities cut at 25% of maximum intensity in order to enhance the visibility of weaker reflections. (B) Diffraction pattern of Kevlar[29] fiber mounted in a stretching cell. The pattern is shadowed at larger angles due to the geometry of the stretching cell.

functions to reflections, a software package based on IDL (*Research Systems Inc.*) was developed.[15] Residual background was treated by a first-order polynomial. Other functions (e.g., Voigtian) will be implemented in the future.

Structural models were based on the Northolt allomorph.[16] The degree of orientation—f_c—of crystallites along the fiber axis (c axis) was derived from the azimuthal broadening of the two strongest equatorial reflections—(110)/(200)—by[7,17]

$$f_c = 0.5[3\langle\cos^2\phi_1\rangle - 1] = 0.5[3(1 - A\langle\cos^2\Phi_2\rangle - B\langle\cos^2\Phi_3\rangle) - 1] \quad (1)$$

with $\Phi = 90 - \phi$, $A = 0.7$, $B = 1.3$, and $\cos^2\phi = [\cos(W_{hkl}/2.35)]^2$ where W_{hkl} is the observed azimuthal width (full width at half-maximum; fwhm) for a specific reflection. Axis 1 is assumed to be the fiber axis —e.g., (002)—, axis 2 corresponds to the (200) reflection, and axis 3 corresponds to the (110) reflection. A and B values are calculated for an orthogonal axis system under the assumption that $\sum\cos^2\phi_i = 1$ which holds for the pseudo-orthorhombic PPTA lattice.[16] As the azimuthal widths of the two equatorial reflections—W_{110} and W_{200}—are below ≈15° one can approximate eq 1 by

$$A\langle\cos^2\Phi_2\rangle \approx A(0.5\pi - [\pi/180°]\langle\Phi_2\rangle)^2 \quad (2)$$

$$B\langle\cos^2\Phi_3\rangle \approx B(0.5\pi - [\pi/180°]\langle\Phi_3\rangle)^2 \quad (3)$$

$$f_c = 1 - \{8.240 \times 10^{-5}(AW_{200}^2 + BW_{110}^2)\} \quad (4)$$

This method of determination of f_c supposes rotational symmetry around the fiber axis, which can be rationalized in the following way. The variation of the intensity of the equatorial (200) and (110) reflections of Kevlar[49] during a linear transversal scan with a 2 μm beam[10] can be simulated by a Gaussian distribution of equatorial planes around the fiber axis of about 56° fwhm.[18] This implies that the crystalline domains of the microfibrils[4] show only weak preferred orientation within the sampled volume. The reciprocal lattice points on the equator will therefore be strongly arced normal to the fiber (c) axis. As the sample is not rotated during the experiments, local fiber symmetry is considered to be a good approximation. f_c values obtained in the present study support this assumption.

A pleated sheet structure with a periodicity of about 0.5 μm along the fiber axis and an angle of 170° between the pleats has been proposed for Kevlar[49] based on electron diffraction

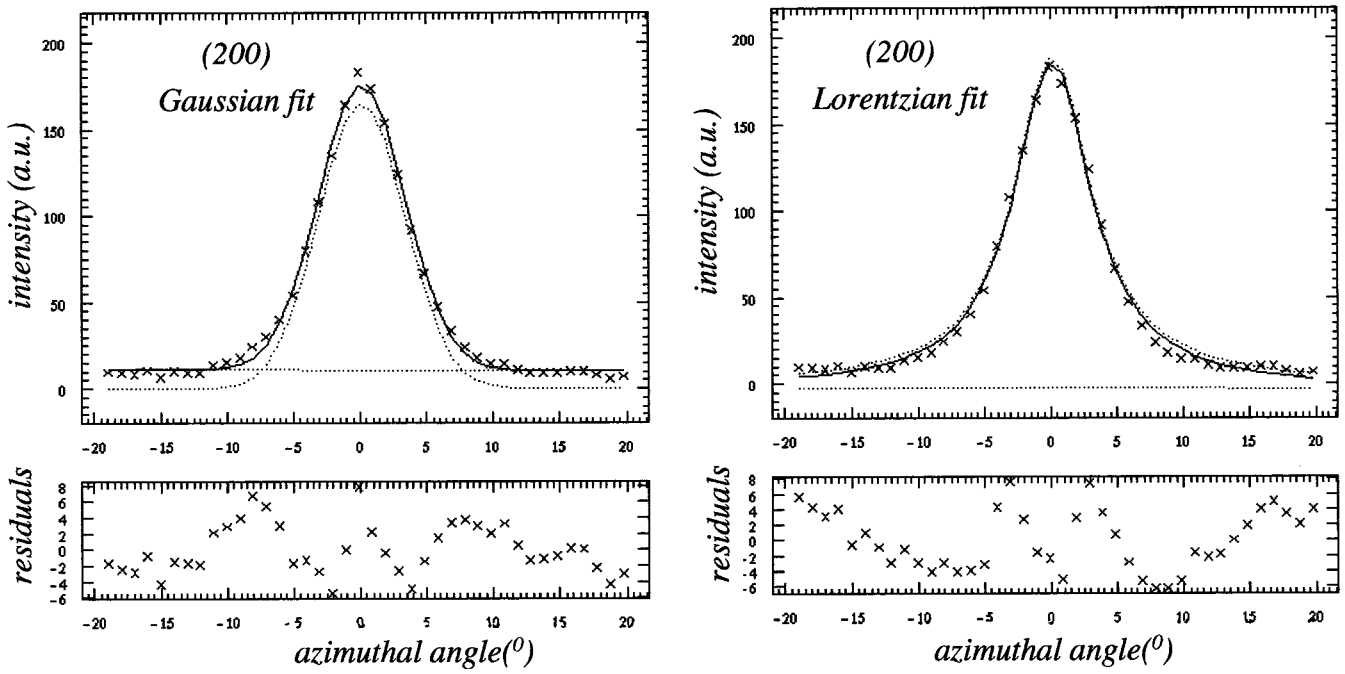

Figure 3. Fit of Gaussian (left) and Lorentzian (right) functions (solid curves) to the azimuthal profile of the (200) reflection of Kevlar[49].

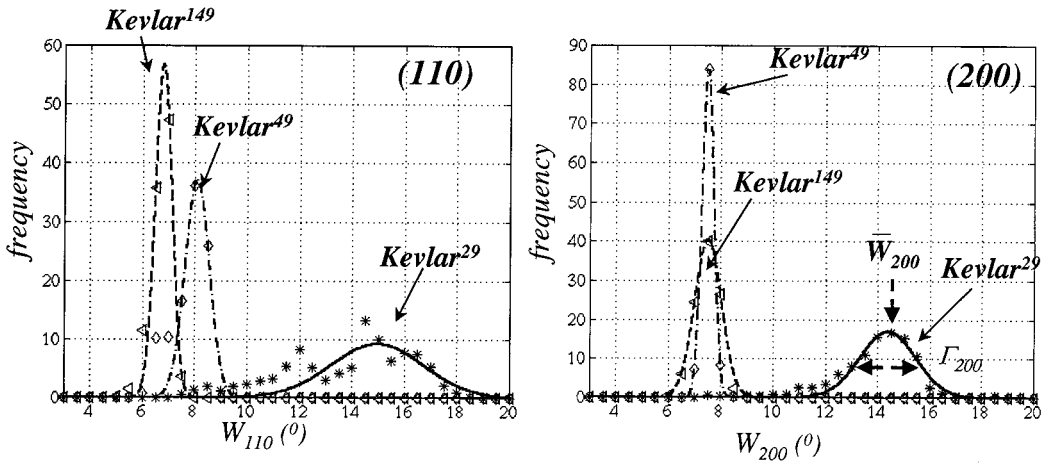

Figure 4. Frequency distribution of azimuthal width (W_{110} and W_{200}) for Kevlar[29,49 149] single fibers. Gaussian functions were fitted to the individual distributions. The definition of the mean azimuthal width ($\bar{W}_{200}$) and its spread (Γ_{200}; fwhm) are shown for Kevlar[29].

techniques.[2,19,20] The sinusoidal undulation of crystallites should result in a corresponding rotation of the diffraction pattern for a scanning experiment along the fiber axis if a beam size of <0.5 μm is used. This assumes a sufficiently regular distribution of pleated sheets in the scattering volume. The 3 μm beam used in the present study will not allow picking up this rotation. It can, however, slightly increase the azimuthal peak width and therefore contribute to the degree of orientation:[2]

$$f_c = f_c^c + f_c^p \qquad (5)$$

f_c^c is due to the distribution of crystallites, and f_c^p is due to the undulations. A quantitative analysis based on the known structural parameters of the pleated sheets is complicated by the lack of information on their volume fraction. The availability of intense submicrometer X-ray beams (e.g., ref 21) should make such structures accessible to scanning microdiffraction and allow a more quantitative analysis of the contribution of the pleated sheets to the diffraction pattern of a single fiber.

Results and Discussions.

A Kevlar[49] pattern recorded in the central part of an unstrained fiber shows the Bragg reflections of the highly oriented pseudo-orthorhombic phase.[16](Figure 2a) In addition to the Bragg reflections, an equatorial streak due to inhomogeneities along the fiber axis is observed.[22,23] Gaussian or Lorentzian functions describe the azimuthal profile of the equatorial reflections reasonably well but show slight deviations in the tails (Figure 3). There was no change in in these deviations and hence the line shape observed during the experiments reported below. To determine the width of the peaks as accurately as possible, a Lorentzian function was initially fitted to the azimuthal profiles radially averaged across the profile, only to determine the center of the reflections. The azimuthal width—W_{110} and W_{200}—(abbreviated in text as $W_{110,200}$) was then obtained by linear interpolation at both sides of the peaks at half of the maximum intensity (fwhm values).

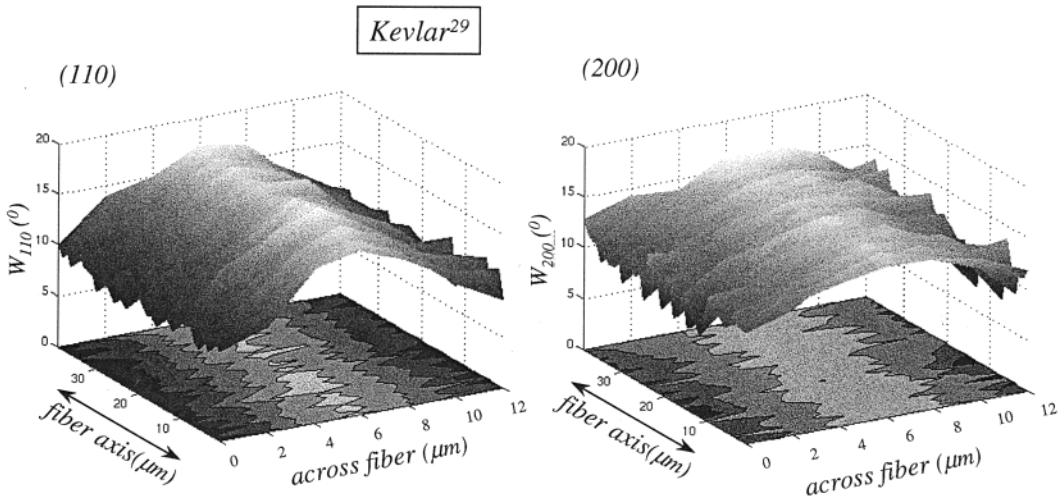

Figure 5. Variation of W_{110} and W_{200} for Kevlar[29] for the mesh of data points.

Table 1. Mean Azimuthal Width ($\bar{W}_{110\,200}$) of (110) and (200) Reflections Determined by Fitting 1D-Gaussian Functions[a]

	$\bar{W}_{110}$ (Γ_{110})	$\bar{W}_{200}$ (Γ_{200})
Kevlar[29]	15.0 (4.1)	14.4 (2.5)
Kevlar[49]	8.1 (1.1)	7.5 (0.5)
Kevlar[149]	6.8 (0.7)	7.5 (1.2)

[a] Spread values (Γ_{110} and Γ_{200}) defined as fwhm of the Gaussian distribution

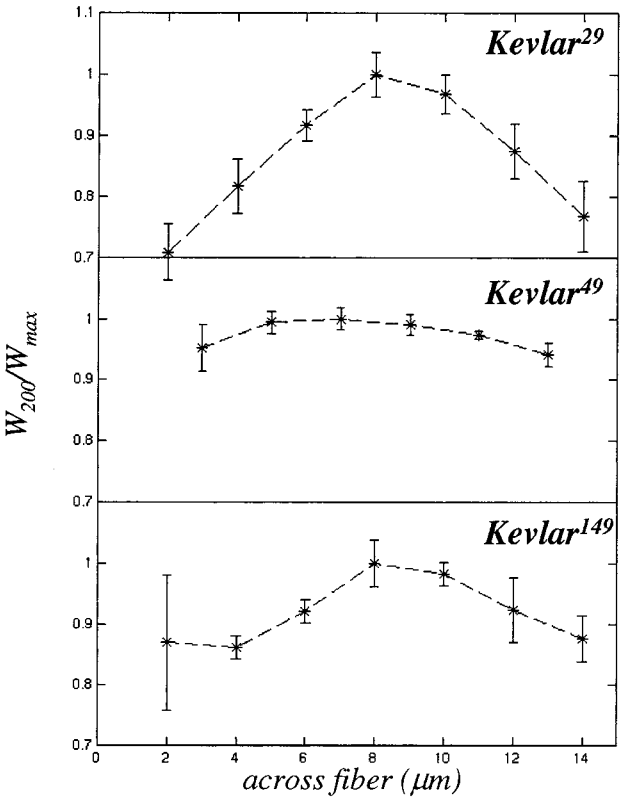

Figure 6. Variation of relative azimuthal width W_{200}/W_{max} (scaled to maximum azimuthal width of (200) reflection $W_{max} = 1$) across the fiber. Values have been averaged along the fiber.

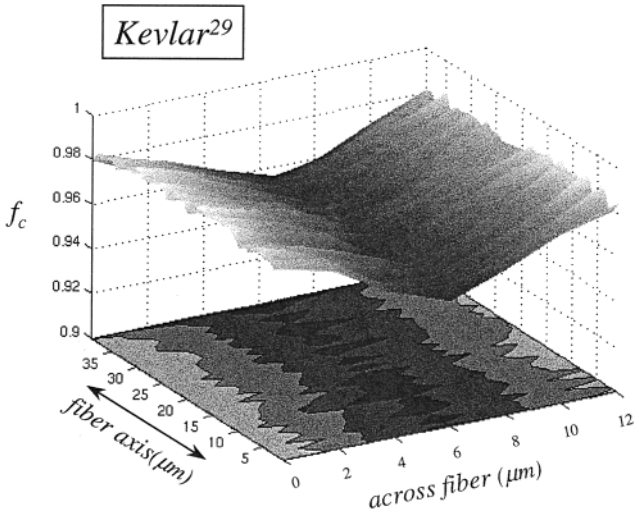

Figure 7. Variation of degree of orientation of crystallites along the fiber axis (f_c) across a Kevlar[29] fiber, calculated from (110) and (200) reflections according to eq 1.

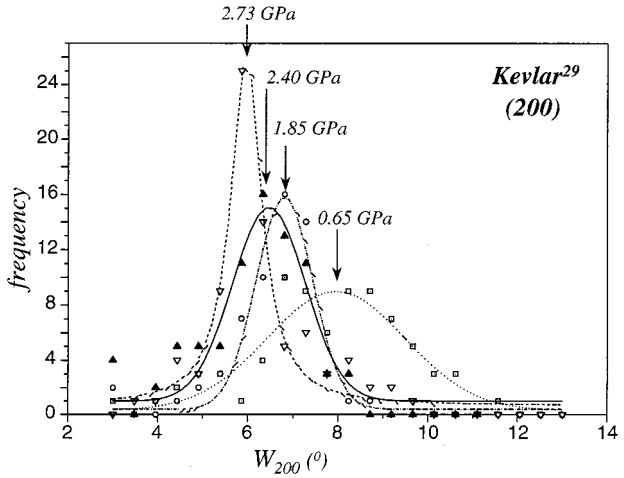

Figure 8. Frequency distribution of W_{200} of Kevlar[29] as a function of applied stress. Gaussian functions fitted to the data points in order to enhance the visibility to the eye.

W_{hkl} values and the corresponding degree of orientation (f_c) derived from one or more fibers with a beam larger than the fiber diameter are already weighted by the contribution from every volume element. The present data were therefore scaled to the scattering volume at every data point in order to obtain comparable values. This was done by determining the relative area of the projection of the fiber onto the fiber-axis intersected by a 3 μm diameter microbeam. The frequency data were then normalized to the values in the middle of the fiber,

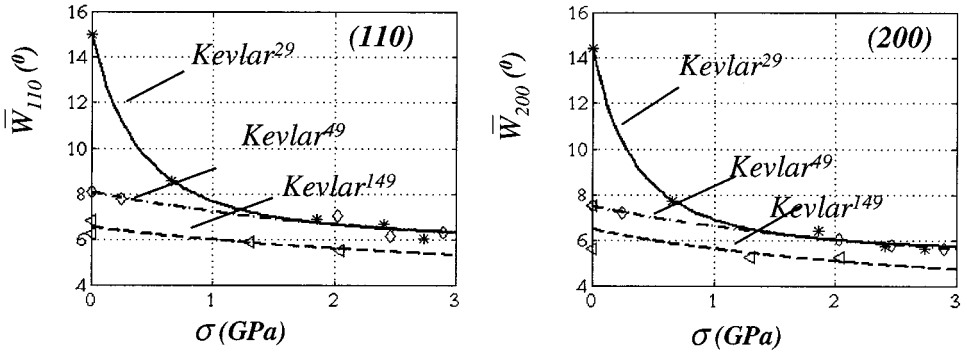

Figure 9. Variation of $\bar{W}_{110,200}$ for Kevlar$^{29,49\ 149}$ as a function of applied stress (σ; GPa). A quadratic function has been fitted to the data (see text).

i.e., at the maximum of scattering volume. The frequency distribution of $W_{110,200}$ values for the three Kevlar samples —corrected in this way—is shown in Figure 4. A Gaussian function has been fitted to every data set in order to determine the mean $W_{110,200}$ values at the center of the function (i.e. $\bar{W}_{110,200}$) and the width of the function (Γ_{110} and Γ_{200}; fwhm), corresponding to the spread of the $W_{110,200}$ values. Values are collected in Table 1. The data show in general a reduction of $\bar{W}_{110,200}$ and $\Gamma_{110\ 200}$ from Kevlar^{29} to Kevlar^{149}. $\bar{W}_{200}$ is, however, the same for Kevlar^{49} and Kevlar^{149}. This suggests that ordering normal to the hydrogen bonded direction (*b*-axis) has reached its optimum value already for Kevlar^{49}. The larger Γ_{200} of Kevlar^{149} as compared to Γ_{200} of Kevlar^{49} suggests that the crystallite orientation is degrading preferentially normal to the hydrogen-bonded planes, possibly due to cross-linking.

The size of the $\Gamma_{110,200}$ values is linked to a gradient of $W_{110,200}$ from the skin to the core of the fibers as shown in Figure 5 for Kevlar^{29}. This gradient is much lower for Kevlar^{49,149} than for Kevlar^{29} as shown for the (200) reflection by plotting the variation of W_{200} (averaged along the fiber axis) across the fiber (Figure 6). It is interesting to note that the gradient seems to be slightly re-increasing from Kevlar^{49} to Kevlar^{149}, which reflects the differences in Γ_{200} observed in frequency space (Figure 4). The present data could be interpreted as a gradual reduction of orientation distribution from skin to core (model I) or as a step function with a better orientation distribution in a skin layer as compared to the core (model II). Assuming a sufficiently thick skin layer for model II, the ratio of core/skin would gradually increase as the beam traverses the sample from the skin to the core. While a skin/core differentiation in PPTA fibers has been reported, there seems to exist no quantitative information on skin/core differences in fibril orientation.[24−26] As the thickness of the skin layer appears to be significantly thinner than 1 μm,[24] its contribution to the azimuthal width can be neglected and one can tentatively assume that model I is more realistic. The origin of the particularly strong transversal gradient in crystallite orientation in Kevlar^{29} is probably due to the fabrication process where the dope is subject to shear stresses in the spinneret capillary, extensional forces in the air gap, and solidification in the coagulation bath.[24] The gradient implies also a gradient in mechanical properties with the modulus decreasing from the outside to the inside of the fiber. Interestingly one observes additional ripples in $W_{110,200}$ along the fiber axis, which overlay the transversal gradient in azimuthal width and will be discussed below.

Table 2. Mean Degree of Orientation, $\bar{f}_c$, along the Fiber Axis Derived from (110) and (200) Reflections[a]

sample	$\bar{f}_c$	f_c[6]
Kevlar^{29}	0.966(22)	0.961(10)
Kevlar^{49}	0.990(2)	0.982(6)
Kevlar^{149}	0.992(3)	0.991(4)

[a] Spread of f_c values from Wu & Blackwell[6] corresponds to measuring statistics, while the spread of the present values (fwhm) reflects the distribution of values across the sampled area of the fiber.

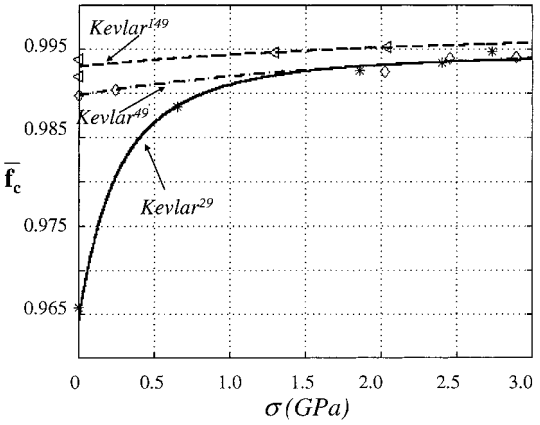

Figure 10. Variation of mean degree of orientation—$\bar{f}_c$—of Kevlar^{29,49,149} as a function of applied stress (σ; GPa).

As expected (see eq 1) the degree of orientation—f_c—of crystallites decreases from the skin toward the center of the fiber as shown in Figure 7. Mean f_c values ($\bar{f}_c$; derived from $\bar{W}_{110}$ and $\bar{W}_{200}$) and the width of the distributions (fwhm) for the different Kevlar fibers are collected in Table 2. With the exception of the value for Kevlar^{49}, which is slightly outside, the values are within the range observed for whole fiber experiments.[6]

Stretching Experiments. W_{200} and Γ_{200} decrease with increasing applied stress (σ) as shown in Figure 8 for the Kevlar^{29}. The same holds for the (110) values. The variation of $\bar{W}_{110,200}$ for Kevlar^{29,49,149} as a function of stress is shown in Figure 9. The attempt was not made to model this curve by an elastic deformation of oriented fibrils as current models assume a homogeneous orientation distribution of crystallites throughout the fiber,[8] which does not correspond to the present results. The data points for a specific (*hkl*) reflection were fitted instead empirically by a quadratic function

$$\bar{W}_{hkl} = a + b/(\sigma + c)^2 \qquad (6)$$

where *a*, *b*, and *c* are constants. The mean degree of

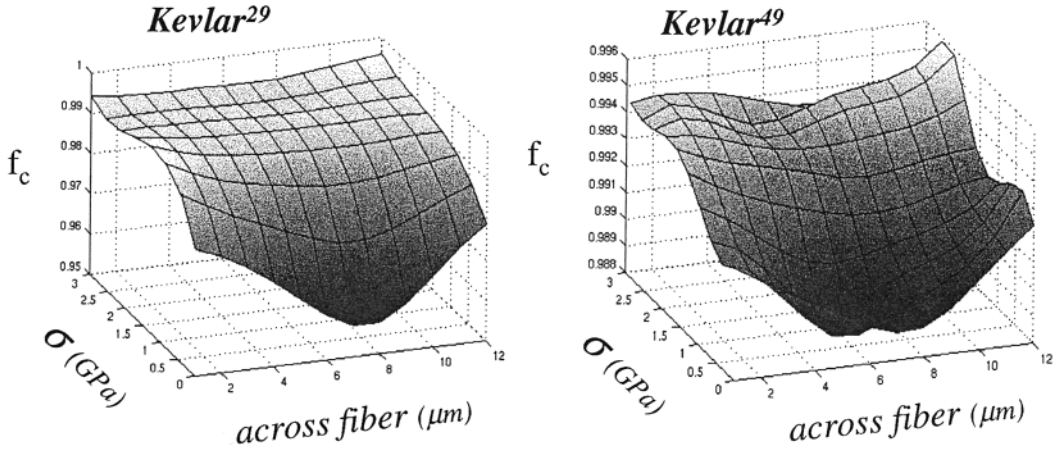

Figure 11. Variation of f_c for Kevlar[29,49] across the fibers as a function of the applied stress (σ; GPa). f_c values are averaged along the fiber axis. Note the difference in f_c scales for the two samples. Grid lines are interpolated between data points (see Figure 10).

orientation—$\bar{f}_c$—as a function of stress is shown in Figure 10. The data suggest that Kevlar[29] reaches the same $\bar{f}_c$ value of Kevlar[49] at about $\sigma \approx 1.5$ GPa. The curves have been calculated from eq 4 by inserting $\bar{W}_{110,200}$ calculated from eq 6. The strong increase of $\bar{f}_c$ in Kevlar[29] up to $\sigma \approx 1.5$ GPa suggests the presence of a frozen-in orientation distribution of crystallites in unstrained fibers, which is no longer existing above about 1.5 GPa. An approach of $\bar{f}_c$ values for Kevlar[29] and Kevlar[49] with increasing stress would also be expected from the stress/strain curves (Figure 1) although the $\bar{f}_c/\sigma$ curve (Figure 10) does not yet have enough data points for a more detailed correlation. Kevlar[149] shows the same trend in $\bar{f}_c$-variation as Kevlar[49] (Figure 10) but has systematically higher $\bar{f}_c$ values, which suggests an additional irreversible orientation process, presumably induced by a combination of heating and stretching. The physical origin might be the straightening out of the pleated sheet structure in Kevlar[149].[2,27] The persistence of the pleating during stretching up to fiber fracture in Kevlar[49] has been observed by scanning electron microscopy.[20] This suggests that the contribution of f_c^p to f_c (eq 5) can only be small. The variation of f_c with σ across the fiber (averaged along the fiber) is shown for Kevlar[29] and Kevlar[49] in Figure 11. The strong f_c anisotropy for Kevlar[29] at low σ values is evident. At the highest σ values, the f_c anisotropy across the fiber has practically disappeared.

The observation of ripples in $W_{110,200}$ and therefore f_c along the fiber axis (Figures 4,6) is intriguing, but a systematic error induced by the repetitive fitting procedure cannot be completely excluded. However, the evolution of these ripples with applied stress (σ) can give a hint as to their physical significance. A relative ripple amplitude—R_a—can be determined for every σ value by

$$R_a = \{[\sum|f_{ci} - f_m|]/n\}/f_m \qquad (7)$$

where f_{ci} is the f_c value at point i, n the total number of points and $f_m = (\sum f_{ci})/n$. R_a was only determined for the most central, 2 μm wide strip along the fiber axis in order to improve the statistical accuracy. As shown in Figure 12, R_a is decreasing for Kevlar[29] with σ to the level of Kevlar[49]. This supports the presence of *orientation* ripples at least for Kevlar[29]. The ripples have a period of several micrometers, which excludes an effect due to pleated sheets.[19,27] Setting aside the possibility of an external force modulating the spinning process, one cannot exclude that these ripples reflect a modulation of orientation along the fiber axis of morphological structures, which are formed from sheared nematic solutions.[28] One would therefore expect that the period and amplitude of the ripples are sensitive to the conditions of the spinning process.

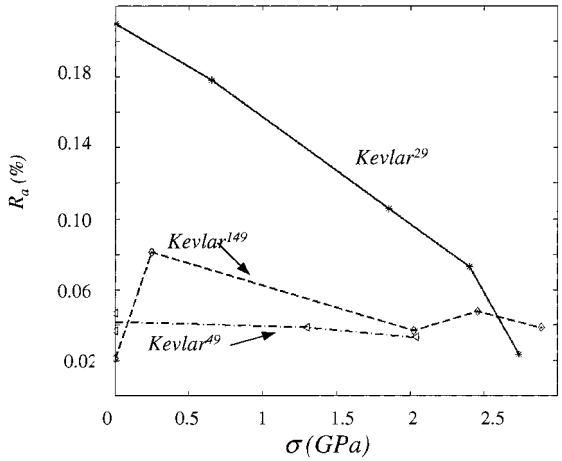

Figure 12. Variation of relative ripple amplitude—R_a—with stress (σ; GPa) for Kevlar[29,49,149].

Conclusions

X-ray scanning diffractometry has been used to study the local orientation along the chain axis of crystallites and therefore of fibrils in single Kevlar[29,49 149] fibers. In general an improvement of fibril orientation from the core to the skin was observed although no evidence for a discrete skin layer was obtained. Kevlar[29] shows the lowest degree of fibril orientation and the strongest gradient, which is presumably due to the fact that the fibrils did not have time to reach an equilibrium orientation during processing. Kevlar[49] and Kevlar[149] do not differ significantly in fibril orientation along the *a*-axis but order along the hydrogen-bonded planes seems to have improved in Kevlar[149]. The gradient in fibril orientation disappears under an applied stress.

The present demonstration experiments are limited to few samples and data points. For the study of finer details of a stress/strain curve and for more routine use, a higher data collection rate will be required. It is feasible to considerably speed up data collection by (i) making improvements in data acquisition (see above) and (ii) using linear scans. Assuming for example four data points for $\Delta\epsilon = 1\%$, one should be able to reach

average strain rates of at least 0.5% min^{-1}. Linear scans would also be of interest for more sensitive fibers as, at every stress level, a scan could be performed on a fresh portion of the sample. Radiation damage could thus be minimized.

Scanning diffractometry can also be applied to map lattice spacings, particle size or small-angle scattering[29,30] across fibers and other samples.

Acknowledgment. The stretching cell used for most of the experiments presented in this text was developed as part of a collaborative project between Keele University (Fuller et al.,) and ICI (Oldman, Eeckhaut) The authors are grateful for the loan of the cell. Support by M. Burghammer (ESRF) and M. Müller (ESRF) is acknowledged. I. Snigireva (ESRF) recorded the SEM data. L.V. is a fellow of the Belgian National Science Fund (FWO).

References and Notes

(1) Kwolek, S. L.; Morgan, P. W.; Schaefgen, J. R.; Gulrich, L. W. *Macromolecules* **1977**, *10*, 1390−1396.
(2) Northolt, M. G.; Sikkema, D. J. *Lyotropic Main Chain Liquid Crystal Polymers*; Höcker, H., Ed.; Springer-Verlag: Berlin, 1991; Vol. 98, pp 115−177.
(3) Jiang, H.; Adams, W. W.; Eby, R. K. In *High Performance Polymer Fibres*; Thomas, E. L., Ed.; VCH: Weinheim, Germany, 1993; Vol. 12, pp 597−652.
(4) Sawyer, L. C.; Chen, R. T.; Jamieson, M. G.; Musselman, I. H.; Russell, P. E. *J. Mater. Sci.* **1993**, *28*, 225−238.
(5) Jackson, C. L.; Schadt, R. J.; Gardner, K. H.; Chase, D. B.; Allen, S. R.; Gabara, V.; English, A. D. *Polymer* **1994**, *35*, 1123−1131.
(6) Wu, T. M.; Blackwell, J. *Macromolecules* **1996**, *29*, 5621−5627.
(7) Northolt, M. G.; Aartsen, J. J. V. *J. Polym. Sci., Polym. Symp.* **1977**, *58*, 283−296.
(8) Northolt, M. G.; Hout, R. v. d. *Polymer* **1985**, *26*, 310−315.
(9) Northolt, M. G. *Polymer* **1980**, *21*, 1199−1204.
(10) Riekel, C.; Cedola, A.; Heidelbach, F.; Wagner, K. *Macromolecules* **1997**, *30*, 1033−1037.
(11) Riekel, C.; Engström, P.; Vincze, L. *Etude Microstructurale des Polymeres par Rayonnement Synchrotron*; G'Sell, C., Ed.; Apollor Edition: Nancy, France, in press.
(12) Martin, C.; Eeckhaut, G.; Mahendrasingham, A.; Blundell, D. J.; Fuller, W.; Oldman, R. J.; Bingham, S. J.; Cunningham, A.; Dieing, T.; Riekel, C. To be published.
(13) Northolt, M. G.; Vries, H. d. *Angew. Makromol. Chem.* **1985**, *133*, 183−203.
(14) Hammersley, A. FIT2D. Website: http://www.esrf.fr/computing/expg/subgroups/data_analysis/FIT2D/index.html.
(15) Vincze, L. Department of Chemistry, University of Antwerp, Unpublished results.
(16) Northolt, M. G. *Eur. Polym. J.* **1974**, *10*, 799−804.
(17) Stein, R. S.; Wilkes, G. L. *Structure and Properties of Oriented Polymers*; Ward, I. M., Ed.; Applied Science Publishers: London, 1975; pp 57−149.
(18) Janotta, A. Trainee project. 1997, unpublished.
(19) Dobb, M. G.; Johnson, D. J.; Saville, B. P. *J. Polym. Sci., Polym. Phys. Ed.* **1977**, *15*, 2201−2211.
(20) Dobb, M. G.; Johnson, D. J. In *Structural Studies of Fibres Obtained from Lyotropic Liquid Crystals and Mesophase Pitch*; Ward, I. M., Ed.; Elsevier Applied Science: London, 1987; Vol. 2, pp 115−152.
(21) Cedola, A.; Lagomarsino, S.; Fonzo, S. D.; Jark, W.; Riekel, C.; Deschamps, P. *J. Synchrotron Radiat.* **1998**, *5*, 17−22.
(22) Dobb, M. G.; Johnson, D. J.; Majeed, A.; Saville, B. P. *Polymer* **1979**, *20*, 1284−1288.
(23) Grubb, D. T.; Prasad, K.; Adams, W. W. *Polymer* **1991**, *32*, 1167−1172.
(24) Morgan, R. J.; Pruneda, C. O.; Steele, W. J. *J. Polym. Sci.: Polym. Phys. Ed.* **1983**, *21*, 1757−1783.
(25) Panar, M.; Avakian, P.; Blume, R. C.; Gardner, K. H.; Gierke, T. D.; Yang, H. H. *J. Polym. Sci.: Polym. Phys. Ed.* **1983**, *21*, 1955−1969.
(26) Horio, M.; Kaneda, T.; Ishikawa, S.; Shimamura, K. *Sen-i Gakkaishi* **1984**, *40*, T-285−T-290.
(27) Krause, S.; Vezie, D. L.; Adams, W. W. *Polym. Commun.* **1989**, *30*, 10−13.
(28) Chen, S.; Jin, Y.; Qian, R. *Makromol. Chem.* **1987**, *188*, 2713−2719.
(29) Müller, M.; Czihak, C.; Vogl, G.; Fratzl, P.; Schober, H.; Riekel, C. *Macromolecules* **1998**, *31*, 3953−3957.
(30) Riekel, C.; Engström, P.; Martin, C. *J. Macromol. Sci.: Phys.* **1998**, *B37*, 587−599.

MA990267M